Materials Today: Proceedings 46 (2021) 658–664

Contents lists available at ScienceDirect

Materials Today: Proceedings

journal homepage: www.elsevier.com/locate/matpr

The microstructure and mechanical properties of the friction stir processed TIG-welded aerospace dissimilar aluminium alloys

Sipokazi Mabuwa *, Velaphi Msomi, Oritanda Muribwathoho, Sharon Saasebeng Motshwanedi

Cape Peninsula University of Technology, Mechanical Engineering Department, Bellville, 7535, South Africa

ARTICLE INFO

Article history:
Received 3 September 2020
Accepted 18 November 2020
Available online 10 January 2021

Keywords:
Microstructure
Hardness
Tensile properties
Fracture surface morphology

ABSTRACT

The AA6082-T651 and AA8011-H14 dissimilar aluminium alloys were utilised in this study. The dissimilar aluminium alloys were joined using tungsten inert gas (TIG) welding technique. TIG welding is the most used welding technique for aerospace engineering applications. However, the joining of dissimilar alloys comes with its drawbacks. The friction stir processing technique comes as a microstructural modifying technique to improve the associated joint defects. The TIG-welded AA6082/AA8011 dissimilar aluminium joints were studied comparatively with the friction stir processed TIG-welded AA6082/AA8011 joints. This was done to investigate the impact of the friction stir processing on the microstructure and mechanical properties of the said TIG-welded joints. The results showed that the application of FSP on the TIG-welded joints resulted in a decrease of minimum grain size of 12.41 to 3.68 μm. The ultimate tensile strength increased from 86.9 to 90.2 MPa. The stir zone hardness also increased from 55 to 68 HV.

Selection and peer-review under responsibility of the scientific committee of the 2nd International Conference on Manufacturing Material Science and Engineering.

1. Introduction

aluminium alloys are known for versatility and applicability with numerous advantages like lightweight, workability, strength, corrosion resistance, low manufacturing and maintenance cost [1,2]. These attractive characteristics make aluminium alloys the most preferred structural materials in many industries like aerospace, automotive and marine engineering. AA6082-T651 and AA8011-H14 are considered aluminium alloys. AA6082-T651 is an Al-Mg-Si alloy consisting of sufficient plasticity for extrusions and contains very high relative strength [3]. AA8011-H14 is an Al-Fe alloyed grade consisting of moderate strength with excellent corrosion resistance, high ductility and a reflective appearance [4]. The AA6082-T651 replaces AA6061 and AA6063 in aerospace engineering applications [5]. There is a growing demand in joining of dissimilar aluminium alloys in many industries including aerospace engineering [6,7]. The dissimilar aluminium alloys can be joined using the fusion and the solid-state welding techniques. The joining of dissimilar alloys comes with drawbacks like the formation of brittle intermetallic compounds, porosities, coarse grains, solidification cracking and thermal residual stresses which results in poor mechanical properties [8,9]. Theses drawbacks affect joint performance negatively. This, therefore, means a processing technique is required to modify the properties of the joint.

The friction stir processing (FSP) is a microstructural modifying technique that can eliminate the defects due to the change in microstructural grain refinement. in doing so improves the hardness of the friction stir processed region [10]. Many researchers also endorse the friction stir processing technique for enhancing the properties of the joint [11,12]. The TIG-welded AA5083-H111 joints were subjected to FSP to study the microstructure and the mechanical properties of the friction stir processed TIG-welded joints comparatively to the TIG-welded ones [13]. The results showed a significant increase in ductility, tensile strength and hardness due to the refinement of the microstructural grains. FSP was employed on the AA6061 and AA7075 dissimilar TIG welded joints to study the effect of the processing parameters on the mechanical properties of the joints [14]. The results revealed that the tensile strength and hardness increased with an increase in tool rotation, while the residual stress was found to decrease with an increase in tool rotation. There is little available literature where the FSP technique is employed to enhance dissimilar TIG-welded aluminium alloy joints. This paper aims to investigate the microstructure and mechanical properties of the friction stir processed TIG-welded joints in comparison to the TIG-welded ones.

* Corresponding author.
E-mail address: sipokazimabuwa@gmail.com (S. Mabuwa).

https://doi.org/10.1016/j.matpr.2020.11.588
2214-7853/
Selection and peer-review under responsibility of the scientific committee of the 2nd International Conference on Manufacturing Material Science and Engineering.

Table 1
Chemical compositions [16,17].

	Mg	Zn	Ti	Cr	Si	Mn	Fe	Cu	Al
AA8011-H14	0.28	0.084	0.016	0.028	0.52	0.46	0.74	0.13	Bal
AA6082-T6	0.6–1.2	0.0–0.2	0.0–0.10	0.0–0.20	0.7–1.3	0.0–1.0	0.0–0.5	0.0–0.1	Bal
ER4043	0.05	0.10	0.02	-	5.3	-	0.8	0.025	Bal

2. Materials and methods

AA6082-T651 and AA8011-H14 aluminium alloy plates with 250 mm × 55 mm × 6 mm dimensions were used in this study. The edges to be TIG welded were prepared into 45° double V butt joints using a milling machine. Three pairs of the dissimilar aluminium plates were utilised. The ER4043 wire filler with a 2.4 mm diameter was used to fabricate the double V-joint. The chemical compositions of the plates and the wire filler are shown in Table 1. Table 2 TIG welding parameters used. A sample of a TIG-welded plate is presented in Fig. 1(a). After the plates were TIG-welded, the joints were friction stir processed (FSPed) using the automated milling machine. The processing parameters were a traversing speed of 60 mm/min, a rotational speed of 1200 rpm, tool tilt angle of 2°. The processing parameters were predetermined in the previous study [11]. The FSP setup for the TIG welded joints is shown in Fig. 1(b). The processing tool used mas made of H13 tool steel. Fig. 1(c) shows the tool with the dimensions of the tool in mm. Two different material positioning was considered, the first TIG-welded plate was friction stir processed with AA6082 on the advancing side of the tool and AA8011 on the retreating side of the tool and vice versa. Fig. 1(d) shows the plate with the friction stir processed TIG welded joint.

Table 2
TIG welding parameters.

Voltage (V)	Current (Amps)	Gas (argon) (L/min)	Travel speed (mm/s)
35	50	25	4.2

The waterjet technology was used to cut the TIG-welded and friction stir processed TIG-welded plates for different specimens for the test analysis considered. The tests include tensile, hardness, and microstructural analysis. The microstructural analysis specimens were cut perpendicular to the welding direction. The specimens were then etched using the Weck's agent as a pre-etch preceded by the modified Keller's agent. The microstructure analysis was performed using the AE2000 Motic metallurgical microscope. The grain sizes were measured using the ASTM E112 standard and the linear intercept technique using the ImageJ software was employed. The ASTM E8M-04 standard was used for

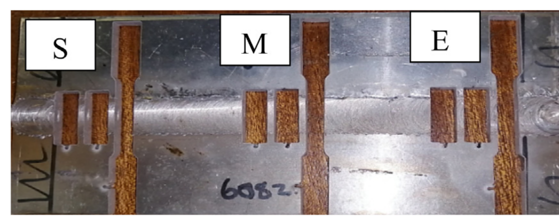

Fig. 2. Specimen positioning.

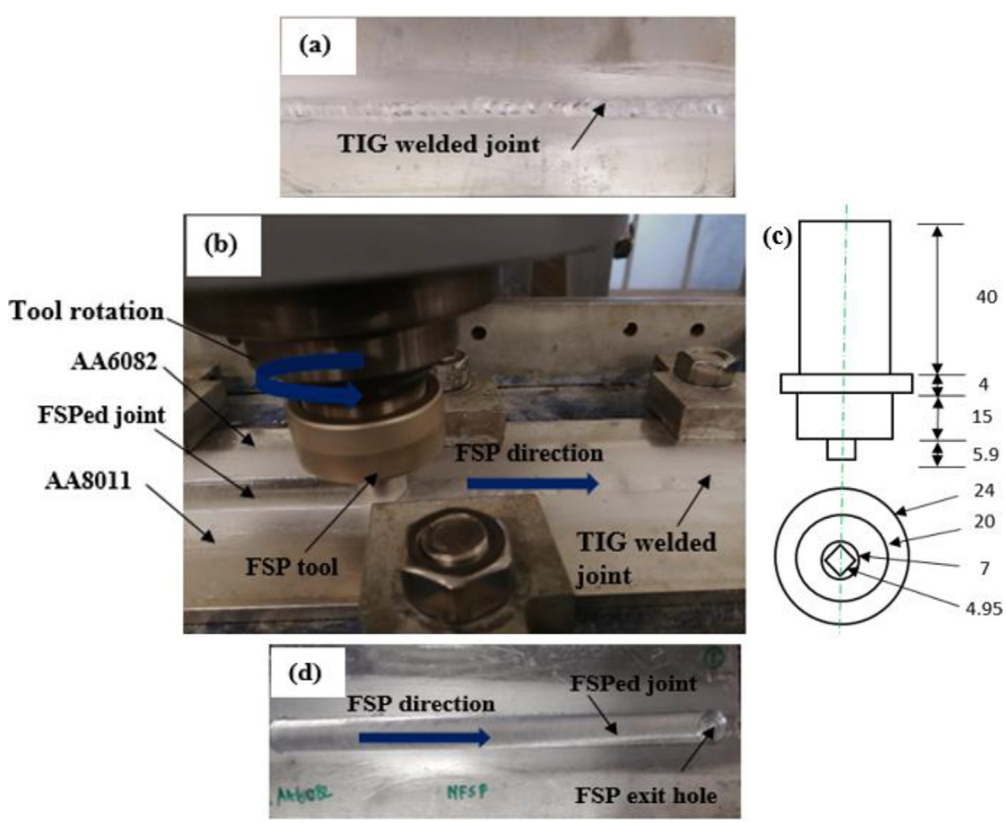

Fig. 1. (a) TIG welded joint, (b) FSP setup, (c) FSP tool, and (d) Friction stir processed TIG-welded joint.

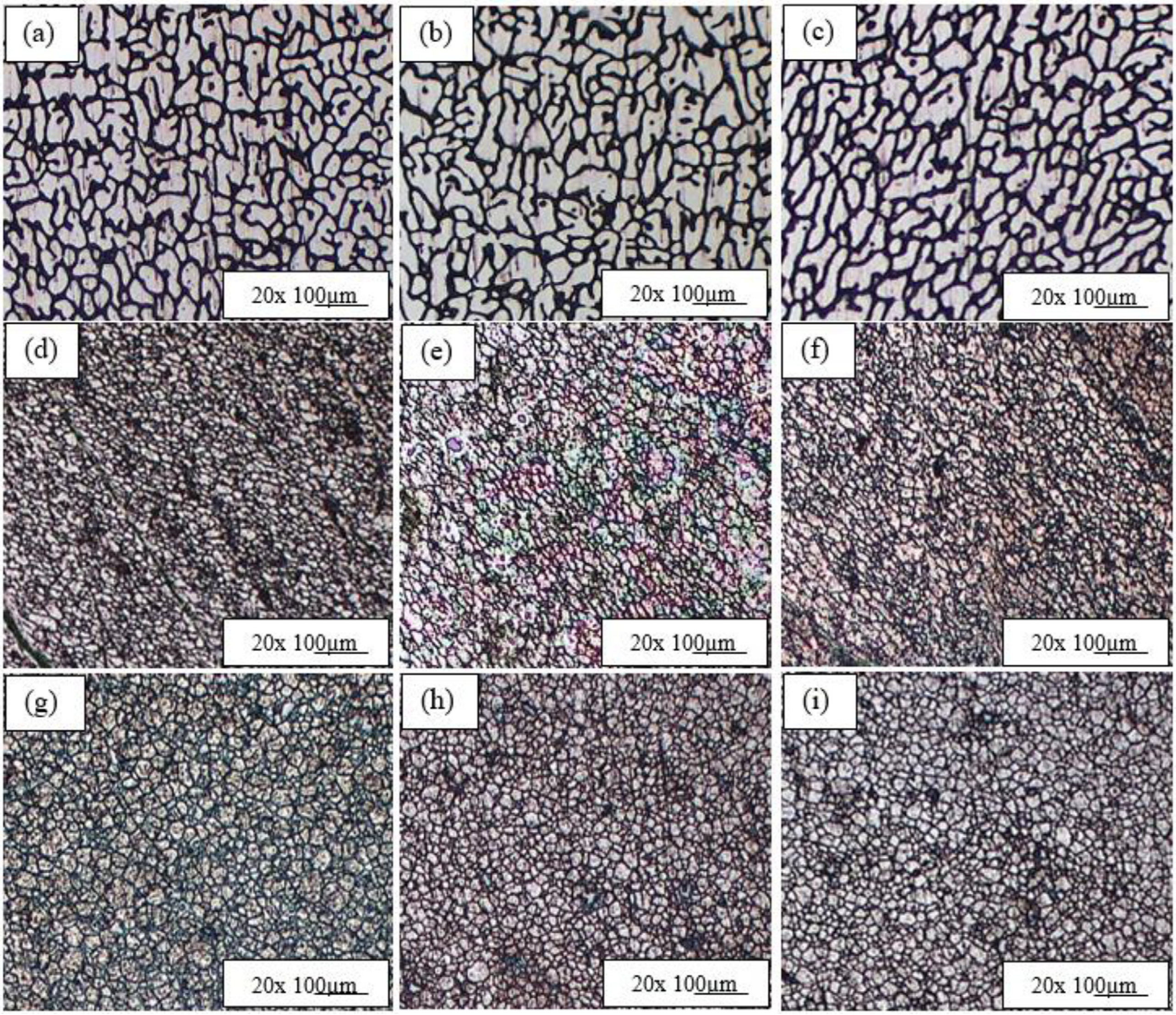

Fig. 3. Micrographs; TIG welded joints, (a) Start, (b) Middle, (c) End; FSPed joints AA6082 advancing (d) Start, (e) Middle, (f) End; FSPed joints AA8011 advancing (g) Start, (h) Middle and (i) End.

Table 3
Summarised stir zone grain sizes.

Joint	Minimum grain size (µm)	Maximum grain size (µm)	Mean grain size (µm)	Standard deviation (µm)
TIG -S	12.41	40.81	22.71	6.46
TIG -M	7.42	39.04	24.59	7.16
TIG -E	10.98	35.88	25.99	7.45
NFSP6A-TIG-S	3.68	16.06	9.25	3.03
NFSP6A-TIG-M	3.78	14.5	9.16	2.55
NFSP6A-TIG-E	3.89	11.86	6.51	1.77
NFSP8A-TIG-S	4.12	16.04	11.03	3.05
NFSP8A-TIG-M	4.34	15.61	9.77	2.96
NFSP8A-TIG-E	4.94	14.08	8.87	2.05

tensile specimen geometry and testing parameters. The tensile test was carried using a Hounsfield H25K universal tensile testing machine. Fig. 1(c) illustrates the tensile test specimen with dimensions in mm. The ASTM E384-11 standard was used for Vickers hardness testing. The 190 HV standard was used for setup. The 0.5 kg load, objective 10x, and 20x were used. The 1 mm interval was used from the centre to either side of the specimen (advancing to retreating). Fig. 2 shows the specimen positioning of the tests conducted, where S, M and E labelling was used. S representing specimens cut toward the start of the joint, M for the middle of the joint and E for specimens extracted towards the end of the joint. This was done to evaluate the impact of the specimen location on the properties of the joints.

3. Results and discussion

Fig. 3 shows the stir zone micrographs of the TIG and friction stir processed TIG-welded dissimilar aluminium alloy joints.

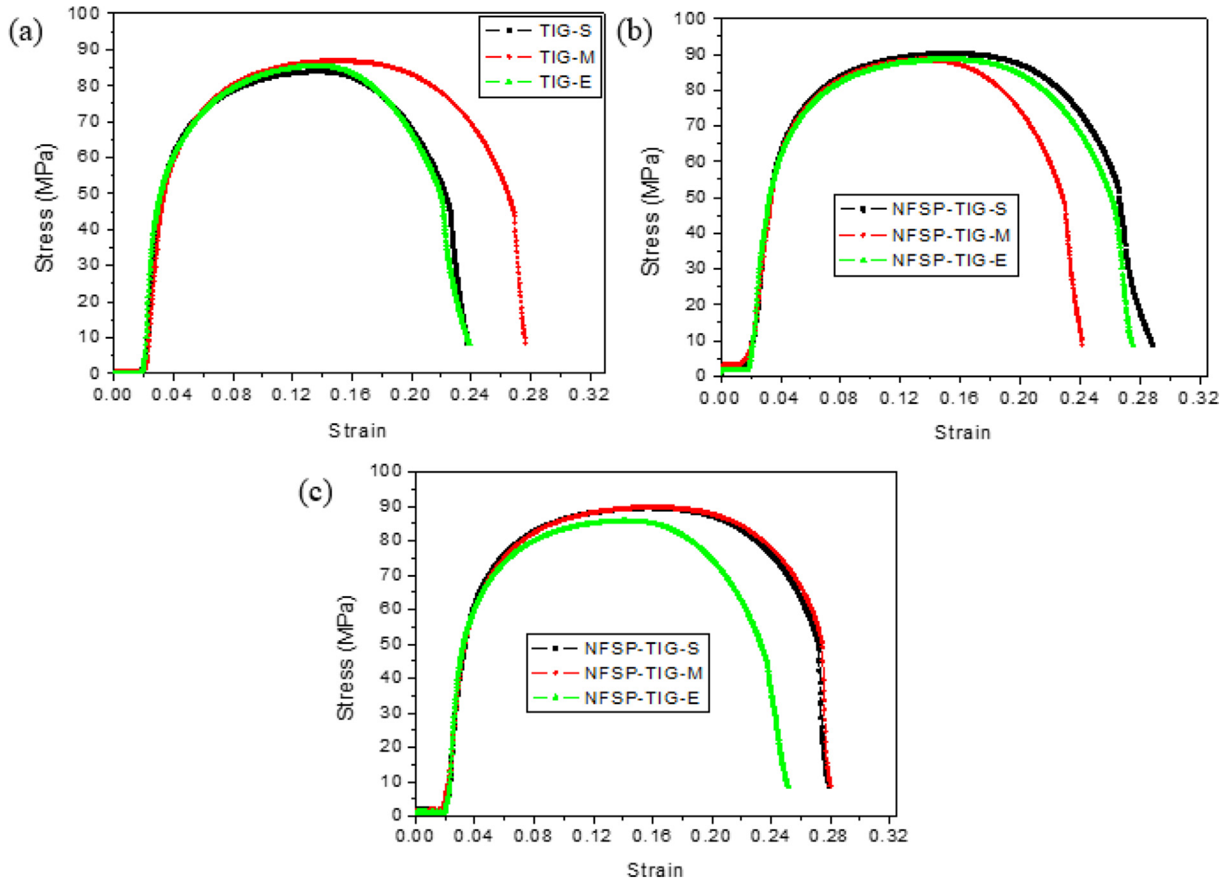

Fig. 4. Tensile curves, (a) TIG welded joints, (b) FSPed joints AA6082 advancing and (c) FSPed joints AA8011 advancing.

Table 3 shows the summarised stir zone grain sizes. Fig. 3(a) to (c) shows the TIG welded grain structure with a mean average grain size ranging from 22.711 μm to 25.99 μm was obtained. Fig. 3(d) to (f) shows the grain structure of the friction stir processed TIG-welded dissimilar joint with AA6082 on the advancing side. The grain size range of the AA6082-AA8011 joint was 6.51 μm to 9.25 μm, with a minimum grain size of 3.67 μm and a minimum standard deviation of 1.77 μm. Fig. 3(g) to (i) shows the AA8011-AA6082 grain structure with a mean grain size range of 8.87 μm to 11.03 μm. The joint had a minimum grain size of 4.12 μm and a standard deviation of 2.05 μm. The friction stir processed TIG-welded joints had finer grain structure compared to the TIG-welded ones. As can be seen on the figure the TIG-welded coarse grain sizes were transformed into finer recrystallized equiaxed grain structures. This transformation of the stir zone was due to the maximum plastic deformation resulting in material softening [15–17]. Similar behaviour was reported in the literature [18].

Fig. 4 shows the stress and strain curves for the TIG-welded and friction stir processed TIG-welded joints with Table 4 tabulating the summarised tensile properties of the joints. From the figure, it was noted that the tensile strain for the friction stir processed joints was higher compared to that of the TIG-welded ones. The maximum tensile strength of 86.9 MPa was obtained for the TIG-welded joints while the friction stir processed ones had maximum tensile stress of 90.2 MPa for the AA6082-AA8011 joint and 89.8 MPa for the AA8011-AA6082 joint. The minimal increase in the tensile strength of the friction stir processed joints was due to the decrease in the grain size [12,13]. The TIG-welded joint had a maximum percentage elongation of 26.91%. The maximum percentage elongation of the friction stir processed TIG-welded joint AA6082-AA8011 was 29.14% and for the AA8011-AA6082 was 27.42%. This improvement of the friction stir processed joints percentage elongation was improved due to the refined microstructural grain sizes, absence of porosities and defects in the joint [10,13]. This behaviour between the microstructure grain size and tensile properties reflects the Hall-Petch relationship [19]. It was noted there was no particular sequence of the results in terms of specimen positioning for both TIG-welded and friction stir processed TIG-welded joints.

Table 4
Tensile properties.

Joint	Tensile strength (MPa)	Percentage elongation (%)
TIG -S	83.9	23.06
TIG -M	86.9	26.91
TIG -E	85.4	23.86
NFSP6A-TIG-S	90.2	29.14
NFSP6A-TIG-M	88.5	23.91
NFSP6A-TIG-E	88.5	26.77
NFSP8A-TIG-S	89.6	27.2
NFSP8A-TIG-M	89.8	27.42
NFSP8A-TIG-E	85.8	24.46

Fig. 5 presents the fracture surface morphology of the post tensile specimens. All the specimens showed a ductile mode of failure. The TIG-welded joints all fractured on the heat-affected side of AA8011 and the friction stir processed joints in Fig. 5(d) and (g) hence the SEM fractographs looks more similar. The ductile features noted in the figures consisted of large, small and torn dimple sizes. Cleavage facets of different sizes were also noted in all the figures. The large dimples and microvoids indicated low ductility, correlating with the respective percentage elongations [20–21]. The friction stir processed TIG-welded joints dimples were found

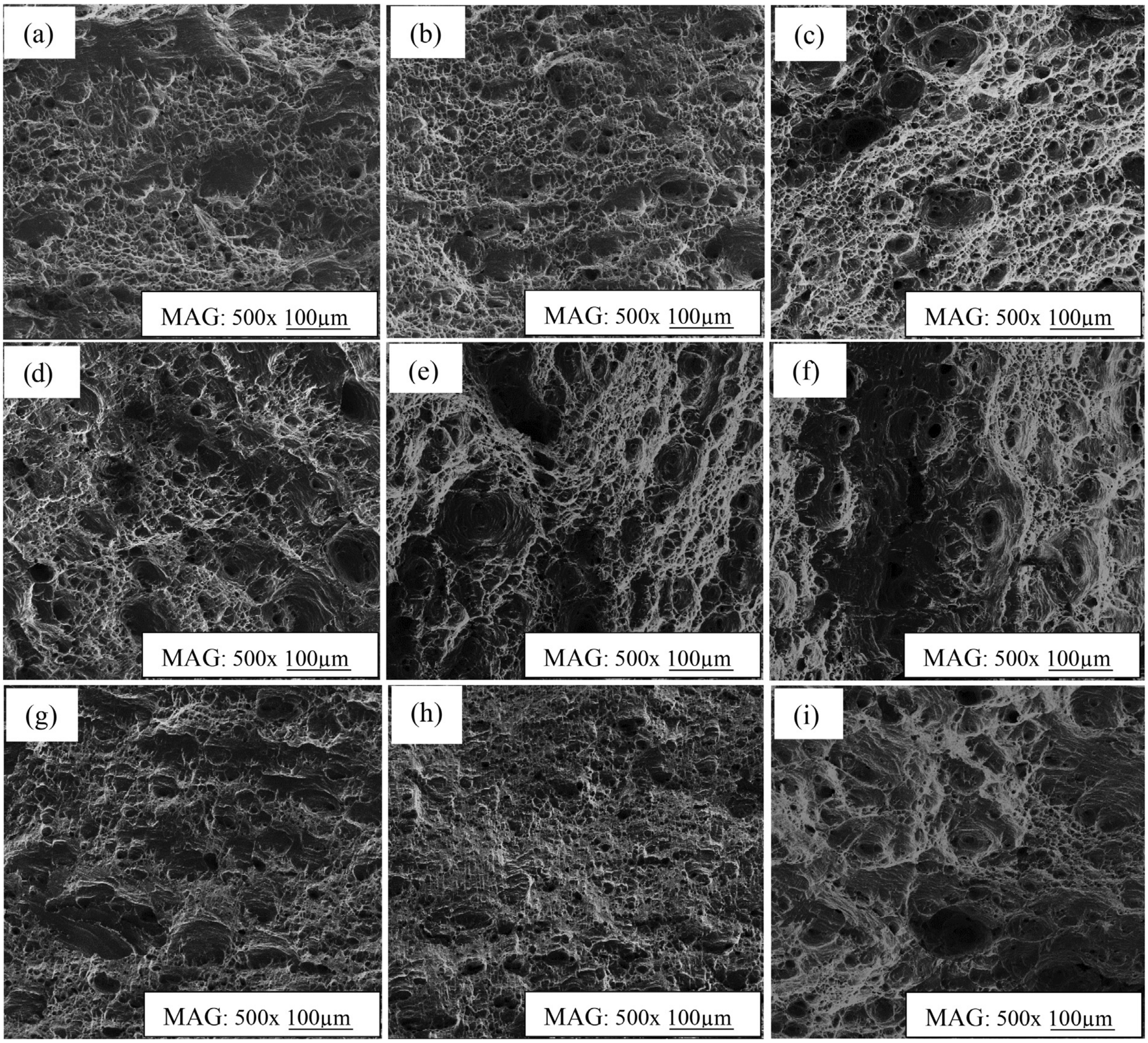

Fig. 5. SEM fractographs; TIG welded joints, (a) Start, (b) Middle, (c) End; FSPed joints AA6082 advancing (d) Start, (e) Middle, (f) End; FSPed joints AA8011 advancing (g) Start, (h) Middle and (i) End.

to be more regular and finer compared to the TIG-welded ones, due to the arrangement of the equiaxed grain sizes and improved mechanical properties [14].

Fig. 6 shows the hardness profiles of the TIG-welded and friction stir processed TIG-welded joints. The hardness results also increased from 55 HV to 68 HV after friction stir processing. The TIG-welded joints showed a stirred zone hardness range of 24 HV to 62 HV, with the specimen extracted from the end of the joint showing the least hardness of 58 HV. The friction stir processed TIG-welded joints with AA6082 on the advancing side showed a hardness range of 23 HV to 60 HV, with the specimen extracted from the middle having the least hardness. The friction stir processed joints with AA8011 on the advancing side showed a hardness range of 22 HV to 68 HV with the specimen extracted from the start of the weld joint having the least hardness. All the maximum stir zones obtained from both TIG-welded and friction stir processed joints were higher compared to the base material of the AA8011 but lower compared to that of the AA6082. This behaviour was due to the AA6082 base material being precipitate strengthened, in which once the joints experienced heat above 200 °C the precipitates disappear [22–23].

4. Conclusions

The investigation on the microstructure and the mechanical properties of the friction stir processed TIG-welded dissimilar aluminium alloy joints were successfully carried out. Friction stir processing has been proven to be able to breakdown the coarse grain structure of the TIG-welded joint into fine equiaxed grain structure through the dynamic recrystallization and plastic deformation experienced by the joints. The friction stir processed TIG-welded joints showed a refined grain structure compared to the TIG-welded ones from a minimum grain size of 12.41 to 3.68 μm. However, the joint AA6082-AA8011 where AA6082 was positioned on the advancing side had much finer grains (3.68 μm) than the AA8011-AA6082 (4.12 μm) one where the AA8011 was positioned on the advancing side. The friction stir processed TIG-welded joints showed better maximum tensile strengths of 90.82 MPa and 89.6 MPa for compared to the 86.9 MPa obtained for the TIG-welded joint. The joint where the AA6082 was positioned showed better tensile properties. As far as the specimen positioning was concerned, there was no particular sequence observed. The ultimate tensile strength increased from 86.9 MPa to 90.2 MPa. The

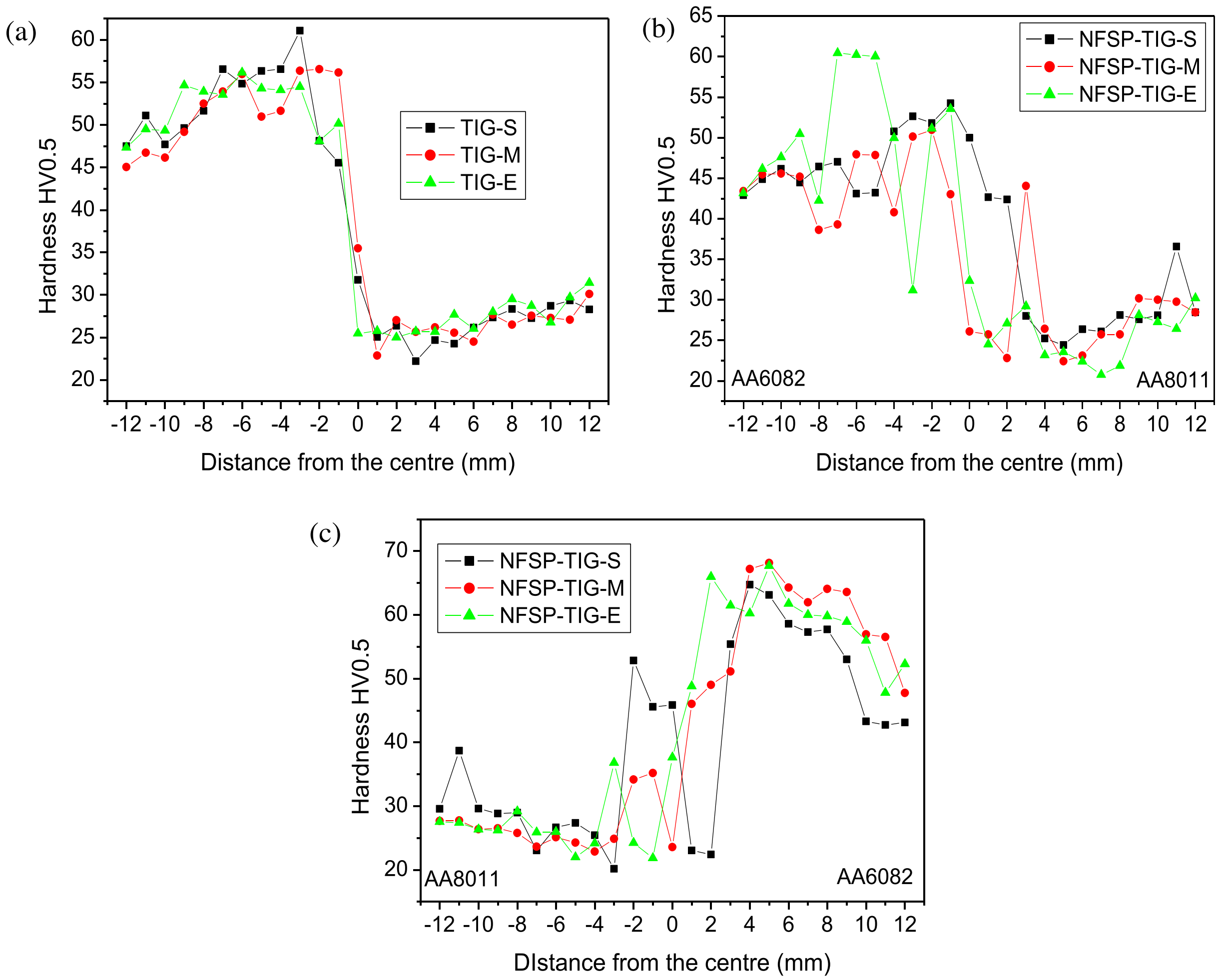

Fig. 6. Hardness profiles; (a) TIG welded joints, (b) FSPed joints AA6082 advancing and (c) FSPed joints AA8011 advancing.

fracture surface morphology results correlated with the tensile results showing the ductility of the specimens. The hardness results also increased from 55 HV to 68 HV after friction stir processing. The positioning of the AA8011 on the advancing side during the friction stir processing of the TIG-welded joints yielded a maximum hardness of 68 HV while with AA6082 a hardness of 61 HV was obtained.

Declaration of Competing Interest

The authors declare that they have no known competing financial interests or personal relationships that could have appeared to influence the work reported in this paper.

Acknowledgements

The authors would like to acknowledge the Cape Peninsula University of Technology mechanical engineering workshop staff especially Mr Mark Jenkins for his assistance with TIG welding and Miss Shaheeda Petersen for her assistance in specimen preparation for the microstructural analysis. Special appreciation also goes Ms Miranda Waldron from the University of Cape Town for assistance with scanning electron microscopy tests.

Funding

The authors would like to acknowledge the National Research Foundation (NRF) Thuthuka Grant for funding this study.

References

[1] T. Dursun C. Soutis Mater. Des. 56 2014 (1980–2015), 862 871.
[2] E.A. Starke Jr., H.M.M.A. Rashed, Mater. Sci. Mater. Eng. 2016 (2016) 18–24.
[3] X. Chen, Y. Peng, S. Peng, S. Yao, C. Chen, P. Xu, J. Pl, PLoS One 12 (7) (2017) e0181983.
[4] J. Fayomi, A.P.I. Popoola, O.M. Popoola, O.P. Oladijo, O.S.I. Fayomi, Results Phys. 14 (2019) 102469.
[5] S. Verma, M. Gupta, J.P. Misra. Friction Stir Welding of Aerospace Materials, B. Katalinic (Ed.), Published by DAAAM International, Vienna, Austria 2016, pp. 135-150.
[6] M. Ilangovan, R.S. Boopathy, V. Balasubramanian, Trans Nonferrous Met. Soc.: China 25 (4) (2015) 1080–1090.
[7] R. Rudrapati, Intec. Open (2019) 1–3, https://doi.org/10.5772/intechopen.89382.
[8] P. Peng, Y. Ma, J. Hu, W. Jiang, Y. Huan, Z. Chen, T. Zhang, T. Adv, Mater. Sci. Eng. (2018) 1–11.
[9] N.M. Daniolos, D.I. Pantelis, Int. J. Adv. Manuf. Technol. 88 (2017) 2497–2505.
[10] H. Mehdi, R.S. Mishra, SN Appl. Sci. 1 (2019) 712.
[11] S. Mabuwa, V. Msomi, Eng. Failure Analysis 118 (2020) 104876.
[12] V. Gopan, P.S. Sreekumar, J.P. Chandran, W. Vijay, M.S. Kumar, Mater Today Proceed. 5 (2018) 13674–13681.
[13] S. Mabuwa, V. Msomi, Adv. Mater. Sci. Eng. (2019) 1–15.
[14] H. Mehdi, R.S. Mishra, Defence Technol. (2020), https://doi.org/10.1016/j.dt.2020.04.014.
[15] D.F.O. Braga, L.M.C. de Sousa, V. Infante, L.F.M. da Silva, P.M.G. Moreira, J. Adhesion 92 (7–9) (2016) 665–678.
[16] M. Balakrishnan, I. Dinaharan, R. Palanivel, R. Sathiskumar, J. Allo. Comp. 78 (2019) 531–541.
[17] G.R. Cui, Z. Ma, S.X. Li, Scri. Mat. 58 (2008) 1082–1085.
[18] H. Mehdi, R.S. Mishra, Metall. Microstruct. Analysis (2020) 1–15.
[19] A. Sanaty-Zadeh, Mater. Sci. Eng. A 531 (2012) 112–118.
[20] K.K.T. Thilagham, S. Muthukumaran, Mater Today: Proceedings (2019), https://doi.org/10.1016/j.matpr.2019.09.228.
[21] P. Cavaliere, A. Squillace, F. Panella, J. Mater. Proc. Technol. 200 (1–3) (2008) 364–372.

[22] A. Barcellona, G. Buffa, L. Fratini, D. Palmeri. J. Mater. Proc. Technol. 177:1–3) (2006) 340-343.
[23] M.D. Sameer, A.K. Birru, J Magn. Alloy 7 (2) (2019) 264–271.

Further Reading

[1] G. Selvaraj, T. Karthikeyan, R. Mohanadass, S. Indhumath, Int. J. Appl. Eng. Res. 10 (13) (2015) 11095–11100.